Title
The Effect of Fungicide Ziram on the hERG Potassium Channel

Permalink
https://escholarship.org/uc/item/4km8h9sz

Author
Kearney, Brian P

Publication Date
2023

Peer reviewed|Thesis/dissertation

UNIVERSITY OF CALIFORNIA

Los Angeles

The Effect of Fungicide Ziram

on the hERG Potassium Channel

A thesis submitted in partial satisfaction of the

requirements for the degree Master of Science in

Physiological Science

by

Brian P Kearney

2023

ABSTRACT OF THE THESIS

The Effect of Fungicide Ziram

on the hERG Potassium Channel

by

Brian P Kearney

Master of Science in Physiological Science

University of California, Los Angeles, 2023

Professor Stephanie Ann White, Chair

Pesticides have been extensively used in agriculture for over a century but concerns regarding their negative impact on human health persist. The relationship between pesticides and human pathogenesis is complex and poorly understood, with myriad factors influencing their effects. Among the health risks associated with pesticide exposure, the development of neurodegenerative diseases, including Parkinson's disease (PD), is of particular concern. The fungicide Ziram has been shown to cause neurotoxicity as well as an increased risk of PD in those who have been chronically exposed. However, the precise mechanism for this effect remains unclear. In the fruitfly *Drosophila melanogaster*, Ziram has been shown to increase neuronal excitability by blocking the ether-a-gogo (*eag)* family of potassium channels. Ziram also increases excitability in mammalian neurons, and we here test the hypothesis that Ziram directly blocks hERG (human eag related gene) potassium channels. Using a non-neuronal cell line expressing hERG we find that Ziram indeed does block this potassium channel. Our data suggest that Ziram acts directly on hERG rather than an accessory subunit.

The thesis of Brian P Kearney is approved.

Barnett Schlinger

Felix Erich Schweizer

Stephanie Ann White, Committee Chair

University of California, Los Angeles

2023

Table of Contents

List of Figures

1. Introduction

Pesticides, valued tools in modern farming practices for over a century, have offered considerable benefits in crop protection and pest control. Yet, their negative impacts on human health present ongoing concerns (Matthews, 2018; Osman, 2011). Particularly affected are vulnerable groups such as migrant farm workers, often at the forefront of direct exposure (Das et al. 2001). The correlation between pesticides, such as Ziram, and human pathogenesis is not fully elucidated, with a multitude of variables confounding the interpretation of potential adverse effects of these chemicals (Mostafalou & Abdollahi, 2013). Among the wide array of health risks posed by pesticide exposure, the incidence of neurological disorders, notably Parkinson's disease (PD), is emerging as a matter of considerable concern (Parron et al. 2011). However, the mechanism of Ziram-associated neurotoxicity remains unclear. Exploring the fundamental interactions between pesticides and neurons can provide insights into novel pathways of idiopathic components of neurodegenerative diseases. Identification of novel pesticide targets, much like known genetic risk factors, might justify comprehensive studies aimed at better understanding and mitigating their involvement in disease. Here we focus on the interactions between the common fungicide Ziram and the human potassium channel hERG.

The human ether-a-go-go related gene (hERG) encodes a potassium channel ubiquitous in various tissues, including the heart, brain, among others. Its primary role is to function as the rapid component of the delayed rectifier potassium current (I_{kr}), a critical contributor to the repolarization phase during an action potential (Perry et al. 2015; Vanderberg et al. 2012). The hERG channel's unique property of voltage-dependent inactivation at highly depolarized potentials distinguishes it from other potassium channels (Sanguinetti et al. 1995; Trudeau et al. 1995). hERG's distinct kinetics during the action potential are first characterized by rapid voltage-dependent activation as the membrane depolarizes, quickly transitioning into an inactivated state, before slowly opening and deactivating during repolarization (Smith et al. 1996). This results in a peculiar "hooked" tail current during repolarization steps in voltage clamp recordings (Shibasaki, 1987), a hallmark of hERG function that is essential for maintaining normal firing rates and rhythm during cardiac and neuronal activities (Chiesa et al. 1997; Perry et al. 2015). hERG is best characterized in the heart due to its association with long QT syndrome when mutated. Mutation of hERG in cardiomyocytes is marked by arrhythmias and sudden cardiac death (Curran et al., 1995; Schwartz, 2008).

The fungicide Ziram has garnered attention due to its association with neurotoxicity and an increased risk of PD in individuals with chronic exposure. Evidence suggests that there is a 3-fold increase in the risk of PD for not only those who are working in fields where Ziram is sprayed, but also in individuals working and living in proximity to those fields (Wang et al. 2011). The physiological mechanism by which Ziram acts as a toxicant in the human body is still not understood (Chou et al 2008; Fitzmaurice et al. 2014; Martin et al. 2016). Notably, there is a

mild association between long QT syndrome and PD (Deguchi et al. 2002). Based on this finding, and the relationship between long QT and hERG mentioned previously, it is clear that hERG is at most a partial contributor to a much more complex pathogenesis, and not a major culprit in the pathogenesis of PD. We hope to show an avenue of physiological inquiry into the broader dysregulation that occurs in PD. In an effort to understand the physiological mechanism by which Ziram increases the incidence of PD, researchers have conducted investigations using the fruit fly *Drosophila melanogaster*. These studies suggest that Ziram induces hyperexcitability in neurons, with a proposed mechanism of this action being that Ziram exhibits a blocking effect on Ether-a-go-go family potassium channels (Harrigan et al. 2021), particularly the seizure (sei) type, which is known to be an ortholog of hERG (Titus et al. 1997).

To address this knowledge gap, we conducted whole cell voltage clamp experiments in HEK cells transfected with the hERG channel. Our preliminary data from electrophysiological recordings suggest that Ziram interacts with hERG, contributing to neurotoxic effects and blocking hERG in a manner similar to what has been proposed in its fruit fly ortholog. Understanding the effect of Ziram on hERG function is crucial for elucidating the mechanisms underlying Ziram-induced neurotoxicity and its association with PD. This research emphasizes the importance of further investigations into the physiological impact of Ziram on the human nervous system and may inform educational and policy changes to protect marginalized populations disproportionately affected by Ziram exposure.

2. Materials & Methods

2.1. Cell Culture

hERG (Kv11.1) - HEK293 Recombinant Cell line (BPS Bioscience, #60619) cells were maintained in Dulbecco's Modified Eagle's medium (DMEM) (1X) (Cat. no. 31966021, Thermo Fisher Scientific, Waltham, MA), supplemented with 10% Fetal Bovine Serum (Cat. no. 16000044, Life Technologies, Carlsbad, CA) and 1% Penicillin-Streptomycin (10,000 U/mL; Cat. no. 15140122, Life Technologies Corp, Grand Islands, NY). Selection was maintained with Geneticin (50 mg/mL; Reference no. 10131-035, Life Technologies Corp. Grand Islands, New York).

2.2. Reagents and Buffer Preparation

The following reagents were used: 0.25% Trypsin-EDTA solution (Cat. no. T4049, Sigma-Aldrich Chemie GmbH, Steinheim, Germany), 1X Ca/Mg Free Phosphate Buffered Saline (PBS) solution(Cat. No. P5493, Sigma-Aldrich, St. Louis, MO), Dimethyl sulfoxide (Cat. no. D8418, Sigma-Aldrich Chemie GmbH, Steinheim, Germany), E-4031 dihydrochloride (Cat. no 113559-

13-0, Tocris Bioscience, Bristol, United Kingdom), and Ziram (Lot no. 7123200, Chem Service, West Chester, PA). The stock solution of Ziram was prepared at a concentration of $10\mu M$. It is important to do this procedure slowly on a vortex to ensure the complete suspension of Ziram in solution. This stock was made weekly, as Ziram oxidizes quickly, thus our preliminary findings suggested that it attenuated Ziram's effect on timescales longer than a week.

An intracellular solution was prepared comprising 135mM K-Gluconate, 0.2mM EGTA, 10mM HEPES, 4mM $MgCl_2$, 4mM Na_2-ATP, 0.4mN Na-GTP, 10mM Na_2-phosphocreatine, and 3mM L-ascorbic acid at pH 7.2 a 290 ± 5 mOsm and stored at -20°C. Aliquoted into 1mL microcentrifuge tubes. On the day of recording, aliquot thawed at room temperature and then kept on ice for the remainder of the experiment. The external bath solution contained 134 mM NaCl, 2.5 mM KCl, 3 mM $CaCl_2$, 1mM $MgCl_2$, 0.34 mM NaH_2PO_4, 1 mM $NaHCO_3$, 20 mM Glucose, and 10mM HEPES at pH 7.30 and 310 $\pm$ 5 mOsm and stored at 4°C. This solution was made fresh every week, and never used longer than 8 days after preparation. On the day of recording, 100mL was warmed in a water bath to room temperature (~21°C) and 0.1% DMSO was added as a vehicle control. For Ziram and E-4031 conditions, 100mL aliquots were thawed and dripped into 100mL external bath solution on a vortex. This was done very slowly to ensure the complete suspension of the compounds in solution.

2.3. Apparatus/Equipment

- 12mm Circle No. 2 micro cover glass (Cat. no. 89015-725, VWR, Radnor PA)
- 35x10mm Tissue Culture Dish (Cat. no. EK-35160, E&K Scientific, Frickenhausen, Germany)
- 1.5mm OD thick-walled borosilicate glass capillaries (Cat. no. Su-BF150-86-10, Sutter Instrument®, Novato, CA)
- Water bath (VWR International, Radnor, PA).
- Everlast™ Rocker 247 (Benchmark Scientific, Sayreville, NJ)
- Vortex Genie 2 (Cat. No. 12-821, Fisher Scientific, Hampton, NH)
- IEC clinical centrifuge (International equipment Co., Needham Heights, MA)
- $25cm^2$ Tissue Culture Flask (Cat. no. 10062-872, VWR, Radnor, PA)
- P-97 Flaming/Brown micropipette puller (Sutter instrument Co., Novato, CA).
- Vapro 5600 Vapor Pressure Osmometer (Wescor EliTech, Logan, UT)
- 70mm filter papers (Cat. no. 1002-070, Whatman, Buckinghamshire, UK)
- accument AE150 Ph Meter (Fisher Scientific, Hampton NH)
- MP-285 Motorized Micromanipulator (Sutter instrument Co., Novato, CA)
- MultiClamp™ 200B microelectrode amplifier (Axon Instruments, Molecular Devices, Sunnyvale, CA).
- 1.5ml Microcentrifuge Tube (VWR, Radnor PA)

- 15 mL Falcon™ conical centrifuge tubes (Cat. no. 14-959-70C, Corning Inc., Brooklyn, NY)
- Forma 5% CO_2 water jacketed incubator (Thermo Scientific,
- Inverted microscope Carl Zeiss Axiovert 200 (Carl Zeiss, Oberkochen, Germany).

3. Procedure

3.1. Preparation of Coverslips

1. Place 30-50 coverslips into a 50mL Falcon Tube, and fill to the top with 1 Molar HCl.
2. Place on Shaker for at least 24 hours.
3. Pour off HCl, and wash 20+ times with DI water.
4. Do 1 final wash with 200 proof ethanol.
5. Prepare a glass petri dish with several layers of filter paper.
6. Place the coverslips onto the layers of filter paper, and autoclave.

3.2 Growth and Maintenance of HEK 293 Cell line

1. Wash cells with 2mL of Ca^{2+}/Mg^{2+} free PBS and aspirate
2. And 1mL of PBS and 100μL of Trypsin and incubate for 5 minutes 37C/5%CO2.
3. With a 1mL pipette triturate cells to detach them from the flask.
4. Transfer to a 10mL tube, add 10-15mL of DMEM.
5. Centrifuge for 5 minutes.
6. Prepare 3 coverslips in a 35mm petri dish, add 3mL of DMEM
7. Prepare 2 small flasks with 5mL DMEM.
8. After centrifugation, vacuum out DMEM from the 10mL tube.
9. Resuspend the pellet in 1mL of DMEM.
10. Count cells, and apply ~5,000 cells per coverslip, and 20,000 per small flask.
11. Split cells when they approach 80-90% confluent.

3.3. Whole Cell Voltage Clamp Recording and Analysis

1. Perform whole-cell voltage-clamp recordings from HEK-293 cells transfected with hERG channel. Using a P-97 Flaming/Brown micropipette puller, make patch-recording pipettes by pulling the pipette from 1.5mm borosilicate glass capillaries.

2. Carefully place one of the coverslips containing the HEK-293 cells in the chamber. Immediately upon placing the coverslip in the chamber, cover with external bath solution using a transfer pipette, make sure the coverslip is fully submerged.

3. Prepare the perfusion system by first clearing the lines with 15mL of DI water, followed by 70% ethanol, and then a subsequent DI wash. Then, fill the external 60 mL syringe with room temperature external bath solution. Ensure that the lines are cleared and running smoothly by allowing 3-5mL of solution to run into a waste container. Make sure that your vacuum apparatus is submerged in solution and that the perfusion is running smoothly at ~1–2 mL/minute.

4. Fill the recording pipette with intracellular solution to approximately half way full. Then hold between thumb and forefinger with the pipette tip facing down. With the other hand, flick the pipette near the tip to release any entrapped air bubbles. Note: be careful to not flick the very tip and thus destroy the pipette. Load the pipette into the holder on your micromanipulator, tighten so that it is airtight. Apply positive air pressure in the pipette using your mouth or a syringe and lower the pipette into the bath. Ensure that the electrode resistance is between 3 and 5 MΩ, if it is not the case being again with a new pipette. Note: Air bubbles prevent closing of the electronic circuit resulting in a high resistance reading, anything from 50 to 1000 MΩ is common. If you see this, discard the pipette and begin again. The internal solution is slightly hypo-osmotic (290 mOsm) as compared to the bath medium (310 mOsm) to facilitate the high resistance seal formation.

5. Find and choose a single healthy cell to patch under the microscope at 10x magnification. Healthy cells tend to look very "plump" and 3D under DIC. Avoid cells that are round and have visible nuclei/vacuoles, this tends to be an indication of a dead or dying cell.

6. Approach the cell and switch to a higher magnification, in our case, 40x.

7. Position your pipette above the cell and somewhere approximately halfway between the center and edge of the cell body.

8. Switch to fine movement on your micromanipulator, and lowly lower the pipette to the cell body. While doing this, make sure to keep the pipette tip in focus, and watch for the cell to begin to come into focus as well.

9. Very carefully watch for a small dimple to form between the pipette tip and the cell membrane, this should also be accompanied by an increase in the pipette resistance (anything from 10 to 100 MΩ is common).

10. At this point you will do the following steps in as rapid succession as possible. First, release the positive pressure, then apply mild negative pressure and lock it into your pipette. Here you should have a rapid increase in the membrane resistance, anything from 100 to 1000 MΩ is common. You have now formed a seal with the cell membrane.

11. Upon achieving a seal, hold the cells at -80mV. Wait 2-3 minutes while the seal stabilizes. If the seal is consistently reading at 1000+ MΩ, then you have formed a Gigaseal. If after stabilization the seal is still not reading at 1000+ MΩ, restart the procedure with a new pipette.

12. Apply sharp bursts of negative pressure until the membrane ruptures, upon doing this you have now achieved Whole Cell confirmation.
13. Begin recording the K+ channel current using a voltage-clamp protocol which consists of a series of 2000 ms long squared voltage depolarizations from -60 to +40mV in 20mV increments. Each trace stepped to -40mV for another 2000 ms, followed by a 1000ms step to -120 after each depolarization before returning to -80mV.
14. Use the Axopatch 200B microelectrode amplifier to investigate the voltage clamp recordings.
15. Analyze the data with LabVIEW PatchClamp software (version 13, Axon Instruments Inc., California, USA) Note: We only used data points that matched our criteria for the analysis and presentation of our findings. Our criteria was that recordings must have at least a 1:10 ratio of Series to Membrane Resistance respectively. Recordings also must have had holding currents not exceeding -200 pA, and these values must have been stable for the entirety of a voltage protocol. Any recordings not meeting these criteria were discarded.

3.4. Data Analysis

One-way ANOVA, Dunn's multiple comparison's test, Linear & Non-Linear Regression, and graphs were performed and made in Prism version 9 (Graphpad inc.). Significance was considered a p-value of < 0.05 and n-values represent the number of biological replicates.

4. Results

4.1. Standard Characterization of hERG in HEK 293 Cells

We first aim to characterize the hERG channel within our HEK cell line, and identify the distinct electrophysiological signatures that are well described in the literature (Vanderberg et al. 2012). Specifically, we hoped to identify a voltage-dependent maximum current followed by decrease at steady state, and the classic "hook" tail current during repolarization. To characterize the hERG potassium channel, we conducted whole-cell voltage clamp recordings in HEK cells (Fig. 1). We next examined the HEK cell endogenous currents in isolation, and thus used a hERG selective channel blocker E-4031. HEK does not endogenously express hERG or any other channel exhibiting voltage-dependent inactivation naturally, and thus we expected to only see the signatures of classical voltage-dependent channels which simply open at depolarized potentials and show no signatures of inactivation or opening during repolarization. We predicted to observe a linear increase in current at increasingly depolarized potentials, as well as no evident tail current. (Fig. 1A) illustrates a stereotypical hERG current, displaying an entire voltage protocol, graphed with the amplitude over time. The voltage clamp protocol used is presented beneath the

graph. This protocol begins at -80mV for 100ms, which was our holding potential for HEK cells throughout our experiments. Next, we depolarized our cells from -60mV to +40mV in steps of 20mV for a duration of 2 seconds. We also repolarized back to -40mV after each depolarization step for another 2 seconds, and then stepped down to -120mV for 1 second before returning to -80mV for 100ms. We designed this protocol to replicate the voltages that a neuron would experience during an action potential, with resting membrane potentials between -70 to -90mV and a peak of the action potential around +40mV. The most important voltage steps for this study are the +40mV, which replicates the peak of an action potential, and -40mV, which simulates the repolarization phase of the action potential. We chose to record repolarization at -40mV and not closer to the -80mV resting potential due to the fact that potassium reversal potential sits around -90mV. Thus, the closer we are to reversal potential, the less potassium current we will see, and we wanted to analyze as robust a hERG current as possible. By clamping the cell to this voltage range, and then systematically depolarizing in a step wise manner, we are able to investigate the voltage-dependent mechanisms of hERG in a way that is near impossible in the millisecond timescales of an action potential. In between each line of the protocol we gave the cell a 10 second rest, as a control refractory period, to recover from the artificially long depolarizations and supposed ion loss. Notably, the characteristic hERG "hook" tail current was observed at -40mV immediately following the depolarizing step.

Next, we investigated the effect of 1μM E-4031, a well-known hERG channel blocker, on the hERG current. If E-4031 is a hERG blocker as described in the literature, then we expect to see no voltage-dependent activation during steady state, and instead a linear increase in current at increasing voltage due to channel recruitment and depolarizations moving further from the reversal potential. We also expect to see a complete eradication of the "hook" tail current in the E-4031 block, as that is a particular signature of hERG not found in any endogenous HEK ion channels. It is evident that the stereotypical hERG tail current was completely abolished in the presence of E-4031 (Fig. 1B). To examine the current-voltage (IV) relationship during our depolarization steps, we plotted the current against voltage for both the control condition and the E-4031 block (Fig. 1C).

The control hERG current showed a characteristic increase in amplitude that peaked and then decreased as the voltage was raised. This peak at $\simeq$+10mVs suggests an equilibrium point between opening and inactivation. Anymore depolarized, and the kinetics favor inactivation over open, thus the decreasing amplitude. In contrast, the E-4031-induced block resulted in a linear increase in current amplitude at steady state with respect to voltage. This is due to the endogenous, voltage-dependent HEK ion channels which are not blocked by E-4031, nor do they feature voltage-dependent inactivation. Thus, at greater and greater depolarization steps, we see greater and greater currents in a linear fashion, following classical channel properties as they move farther and farther from their reversal potential.

7

Next we wanted to identify the amount of hERG current being expressed by our cell line. As was described previously, the literature indicates that hERG only opens and allows current to flow after it has been "primed" by voltage dependent inactivation at depolarized potentials. Only after being inactivated and then undergoing repolarization can hERG open before going through slow closing kinetics, producing the characteristic "hook" tail current. To analyze this property, we assessed the IV relationship during repolarization to -40mV following each depolarization step (Fig. 1D). In the control condition, the amplitude of the hERG current increased and then reached a plateau even as the voltage increased. This is simply due to the fact that around +30mV all of the hERG channels have been recruited, and even at more depolarized potentials, there are simply no more channels to recruit. Conversely, the E-4031 block exhibited no significant change in amplitude relative to voltage, with the amplitude never exceeding 50 pA. This confirmed previous findings that E-4031 exhibits a full block at 1μM. These results provide a comprehensive characterization of the hERG channel's behavior, demonstrating its characteristic tail current, susceptibility to E-4031 block, and the distinct IV relationships during both depolarization and repolarization. These findings serve as a foundation for further investigations into the pharmacological modulation of hERG currents and their role in cellular excitability.

4.2. Ziram's Effect on hERG Tail Current

Here we investigated the effect of Ziram on the hERG potassium channel through whole cell voltage clamp recordings. Our data represents the peak amplitude in pico amps of hERG tail current recorded immediately following a +40mV depolarizing step, recorded at -40mV. We examined the blocking effect of Ziram on hERG at concentrations of 0.5, 1, 1.5, and 2 μM. We recorded no concentrations higher than 2μM, due to the fact that any higher concentration was immediately toxic to the cells, thus rendering patch clamp analysis impossible. We identified this toxicity by the fact that cells would not hold stable seals, and patch clamp would fail spontaneously. This speaks to the fact that the cell membrane integrity was failing, a common feature of cell toxicity. This was further corroborated by the fact that under light microscope our cells would soon after begin to die, spilling their contents into the bath solution. We also recorded 1μM E-4031 for a control block condition, as E-4031 is a well described hERG open channel blocker (Kamiya et al.; 2006; Wang et al., 1997).

Our findings reveal a significant inhibition of hERG tail currents in the presence of 2μM Ziram that was almost identical to that of 1μM E-4031, but none of the other Ziram conditions had a significant effect (Fig. 2A). This reduction in the peak amplitude of hERG currents when in the presence of Ziram indicates a blockade of channel activity. To confirm Ziram's action on hERG, and to rule out any effect of our vehicle, we conducted control experiments using vehicle control in the form of 0.1% DMSO, which was used to solubilize Ziram and at the same 0.1% concentration in all Ziram conditions. This control condition did not result in a significant

8

alteration of hERG currents, suggesting that the observed effects were specifically attributed to Ziram. However, we did notice a large amount of variability in the control condition peak amplitude across our recordings. To assure that this was natural variation such as levels of hERG channel expression, we analyzed our control condition for batch effect (Fig. 2B) as follows.

We began each day of whole cell patch clamp by first recording in control conditions before moving on to our experimental conditions. Although there was considerable variation in control recordings from day to day, we see that there was not significant batch effect. (Fig. 2B). This suggests that the individual coverslip and the time post cell split did not meaningfully affect our results. Finally we analyzed the data to determine a dose response curve (Fig. 2C). Here we see the unusual blocking characteristics in more detail. First, we see that in 0.5 and 1µM conditions there is little in the way of blockade on hERG. Interestingly, we see that there is a slight dip at 0.5µM that then corrects at 1µM. Next we see a drastic drop in amplitude at 1.5µM and then the near total block at 2µM, with the amplitude down to the level of noise, similar to what we had seen in E-4031. This data did not fit a classic sigmoid dose response curve during non-linear regression, but something that appears almost linear. We believe that with more conditions we would have a better sigmoid fit. This curve suggests that the IC50 for Ziram is approximately 1.5-1.7µM, but more conditions will be necessary to resolve the dose response curve at a higher fidelity and determine a more exact number. Taken together, our results demonstrate that Ziram exhibits a potent blocking effect on the hERG potassium channel at a concentration of 2 µM. This blockade is evident through the significant reduction in peak amplitude of hERG currents. These findings suggest that Ziram-induced hERG inhibition may have implications for cellular repolarization processes and potentially contribute to the neurotoxic effects associated with chronic exposure to the fungicide Ziram.

4.3. Ziram's Effect on Voltage Dependent Activation of hERG

An essential electrophysiological property of any voltage-gated ion channel is its current-voltage (I-V) relationship, as previously described (Fig. 1). Examining this relationship can reveal fundamental channel characteristics and provide insight into its broader physiological role. In this section, we delve into the I-V properties of the hERG tail current to assess the channel's voltage-dependent activation. Knowledge of these activation dynamics is crucial to understanding the physiological processes related to cellular excitability and establishing the role Ziram may have in neurotoxicity and Parkinson's Disease pathogenesis (Butler et al. 2020; Nakajima, 1999; Su et al. 2009). Prior studies suggest that Ziram enhances excitability at neuro-muscular junctions in Drosophila Melanogaster (Harrigan et al. 2021; Martin et al. 2016).

We sought to identify a significant shift in the voltage at which the cell attains 50% of its peak tail current amplitude in Ziram conditions versus control (Fig. 3). We normalized the total current proportion in this figure due to the known attenuation of tail current amplitude in Ziram

conditions (Fig. 1). Although our data did reveal a slight reduction in the 50% IMax between control and Ziram conditions, statistical analysis suggests that this change is not significant. These preliminary findings, therefore, imply that Ziram does not substantially alter the activation kinetics of the hERG channel.

4.4. Ziram's Effect on the Tail Current Decay Time Constant

Here we investigate the decay time constant tau (τ) of the hERG tail current. The decay time constant can be used to indicate how quickly an exponential curve decays (Kamyia et al. 2001). In this case, the rate at which the tail current, following a 40mV depolarizing voltage step, returns to baseline. Understanding the characteristics of the decay time constant provides valuable insights into the kinetics of hERG channel deactivation, shedding light on the precise regulation of potassium currents and their impact on cellular excitability. Through whole-cell electrophysiological recordings, we examine the decay time constant of the hERG tail current under various experimental conditions, including 4 concentrations of Ziram as well as the control block E-4031. Here we see a significant decrease in tau at 2uM, but none of the other Ziram conditions (Fig.4A). We also see that this decrease is very similar to the effect of E-4031 on hERG, which is a well characterized open channel blocker (Wang et al., 1997). To confirm that this Ziram-induced decrease in tau was due to effects on hERG deactivation characteristics, and not simply a factor of the decreased amplitude as described previously (Fig. 1A) we analyzed our control data to determine if there is a significant relationship between tail current amplitude and tau (Fig. 4B). Here we plotted tau against the tail current amplitude and then ran a linear regression in order to determine if there was any significant relationship. Thus, we determined that there was no significant relationship between tail current amplitude and tau. This suggests that the effect we see in the 2μM Ziram condition is due to Ziram's interaction with hERG deactivation and not simply that it is greatly attenuated tail current amplitude.

5. Discussion

In this study, we investigate the effect of the fungicide, Ziram, on the hERG potassium channel through whole-cell voltage clamp recordings. We examine the blocking effect of Ziram on hERG tail currents at concentrations ranging from 0.5 μM to 2 μM. Additionally, we included a control condition using the well-characterized hERG open channel blocker, E-4031, at 1μM concentration (Kamyia et al., 2006). Our results demonstrate a significant inhibition of hERG tail currents in the presence of 2 μM Ziram, which was comparable to the effect of 1 μM E-4031. This reduction in the peak amplitude of hERG currents indicates a blockade of channel activity specifically attributed to Ziram.

To confirm the specificity of Ziram's action on hERG, we conducted control experiments using vehicle only (0.1% DMSO) at the same concentration used in all Ziram conditions. The vehicle control did not produce a significant alteration of hERG currents, indicating that the observed effects were specific to Ziram. We also analyze the control condition for potential batch effects and found no significant variation across different recording sessions, suggesting that the observed differences were not due to experimental variability.

Furthermore, we analyze the data to determine a dose-response curve for Ziram's blocking effect on hERG. Our results reveal an unusual blocking characteristic, where lower Ziram concentrations (0.5 µM and 1 µM) showed minimal blockade, a slight dip at 0.5 µM, followed by a drastic drop in amplitude at 1.5 µM and near-total block at 2 µM. These findings suggest that the half-maximal inhibitory concentration (IC50) for Ziram is around 1.5-1.7 µM, which we derived from the line of best fit. Compared to an IC50 of 16nM for E-4031 and 10µM for disopyramide, a class A1 antiarrhythmic drug (McPate et al., 2006). Our IC50 is a rough estimate, and further experiments including Ziram conditions between 1 and 1.5µM as well as 1.5 and 2µM are necessary to obtain a more precise dose-response curve.

Next, we explore the rate voltage-dependent activation of the hERG tail current to understand the channel's activation kinetics in the presence of Ziram. We analyze the voltage at which the cell reached 50% of its peak tail current amplitude in Ziram conditions compared to the control (Su et al., 2009). Although there was a subtle decrease in the 50% IMax between control and Ziram conditions, statistical analysis indicates that this change was not significant. These preliminary findings suggest that Ziram does not markedly shift the activation kinetics of the hERG channel.

In addition, we investigate the decay time constant tau (τ) of the hERG tail current to understand the deactivation kinetics of the channel. Our results demonstrate a significant decrease in tau at 2 µM Ziram, similar to the effect of 1µM E-4031 on hERG, a well-characterized open channel blocker (Wang et al., 1997). This similarity in deactivation kinetics suggests that Ziram and E-4031 may have similar interactions with hERG. Importantly, our analysis shows that the decrease in tau was not solely due to the attenuated tail current amplitude in the Ziram conditions, as there was no relationship between tail current amplitude and tau in our control conditions. These findings indicate that Ziram directly affects the deactivation characteristics of the hERG channel. Further experiments are needed to determine the exact binding characteristics by which Ziram interacts with hERG, but these findings may suggest that Ziram acts as an open channel blocker similar to E-4031.

Taken together, our results provide valuable insights into the blocking effect of Ziram on the hERG potassium channel. The significant inhibition of hERG tail currents, the sharp dose-response, and the impact on the decay time constant suggest that Ziram-induced hERG inhibition may have implications for neuronal repolarization and broader scale electrophysiological processes, and contribute to the neurotoxic effects associated with chronic exposure to Ziram.

Additionally, our findings contribute to the comprehensive understanding of hERG channel function, shedding light on its broader physiological role in the nervous system and its involvement in pathological conditions such as cardiac arrhythmias and neurodegenerative disorders.

These novel insights into the blocking effect of Ziram on the hERG potassium channel hold significant implications for educational and policy changes aimed at protecting those at the highest risk of chronic exposure, particularly migrant farm workers and residence of the Central Valley of California (Luo & Zhang 2010; Ritz & Yu, 2000). Despite being marketed and sold as a relatively safe compound, our findings challenge this perception. It is crucial to educate individuals with the most frequent and prolonged exposure to Ziram about the associated risks, giving them agency over their own wellbeing and allowing them to take appropriate precautions to safeguard their health. Furthermore, from a policy standpoint, we advocate for increased regulation or even a complete ban on the use of Ziram, akin to the actions taken against DDT in the 1960s (Carson, 1962). These measures would prioritize the well-being of vulnerable populations and foster a safer working environment for those involved in agricultural practices.

In summary, hERG is a potassium channel that plays a vital role as the I_{kr} in various tissues including the brain, and its unique voltage-dependent inactivation property distinguishes it from other potassium channels. Here we show that the fungicide Ziram blocks hERG similarly to its proposed interaction with the fly ortholog *sei*. Furthermore, Ziram's blocking and decay characteristics are similar to that of the open channel blocker E-4031, suggesting that Ziram may block hERG in a similar way. However, future investigation is needed to confirm this proposed mechanism of Ziram block. These novel findings provide valuable insights into the potential mechanisms underlying Ziram-induced neurotoxicity and increased risk of Parkinson's disease. We hope to highlight the significance of further research in this area, as well as educational and policy changes which can help protect the marginalized individuals who are disproportionately affected by Ziram.
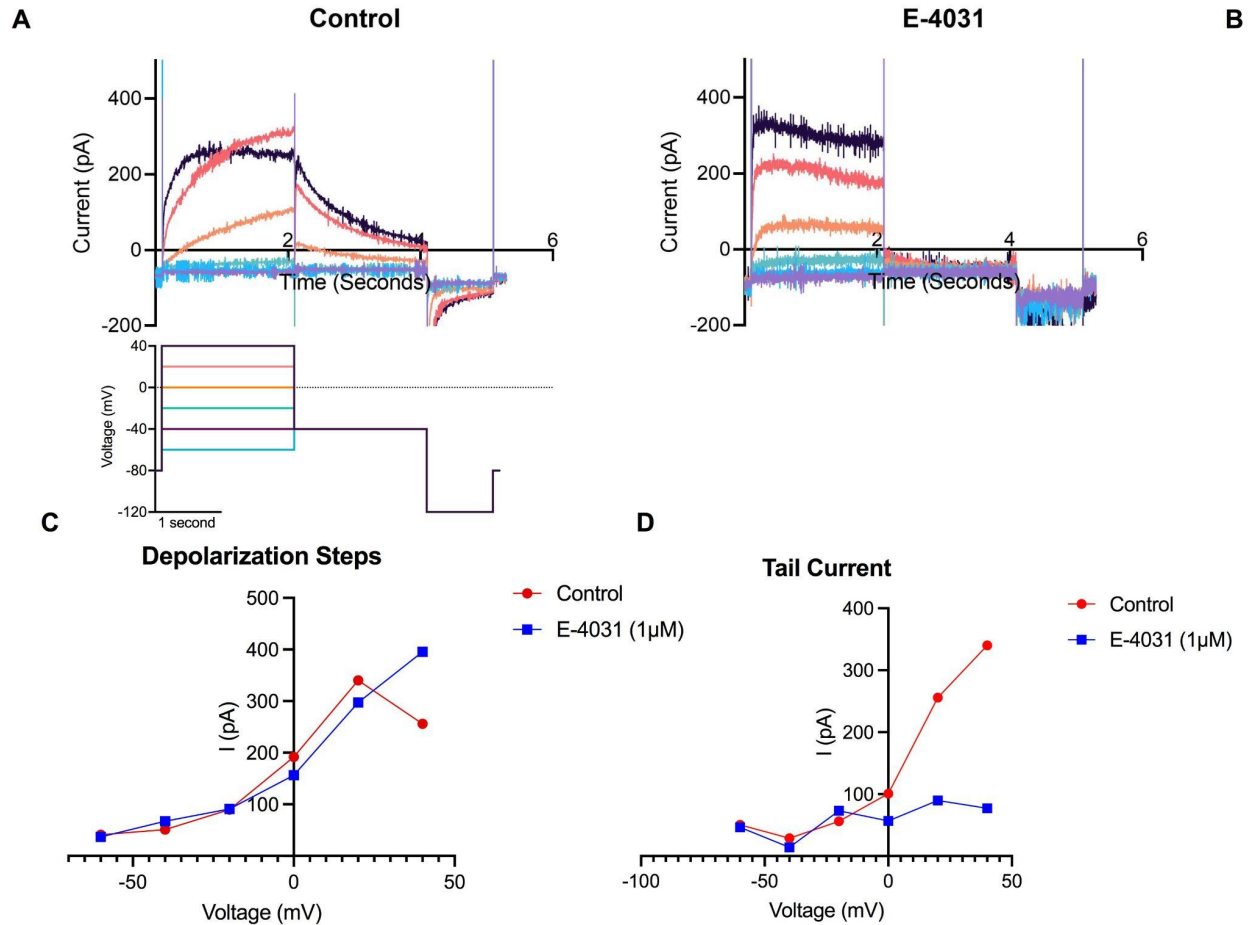
Figure 1. Normal characterization of hERG channel. (A) Amplitude vs Time graph depicting a stereotypical hERG current recorded from a HEK cell. The voltage clamp protocol is depicted underneath. Note the "hook" tail current recorded at -40mV just after 2 seconds. **(B)** Amplitude vs Time graph depicting a stereotypical 1μM E-4031 hERG channel block recorded from a HEK cell. Note the complete absence of the stereotypical hERG tail current. **(C)** IV graph depicting the relationship between current and voltage during the depolarization steps depicted below figure 1.A. Note that E-4031 amplitude continues to increase linearly while the control peaks and decreases. **(D)** IV graph depicting the relationship between current and voltage during the repolarization to -40mV following each depolarization step depicted below figure 1.A. Note that the control amplitude increases and then plateaus while the E-4031 amplitude shows no meaningful change in relation to voltage.
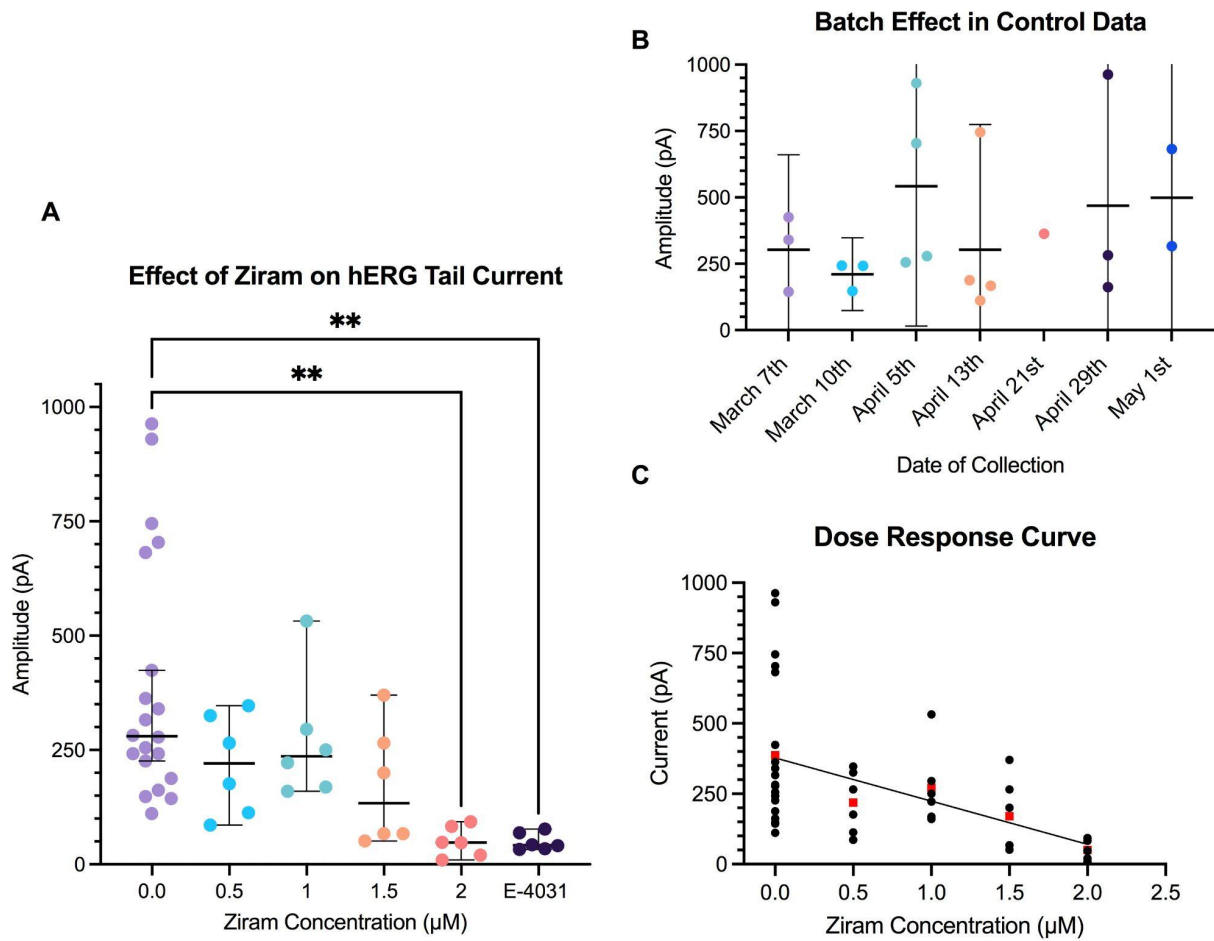
Figure 2. Ziram blocks hERG's tail current. (A) 2uM Ziram significantly blocks the hERG channel tail current (n=6) in comparison to control (n=20) and almost identically to hERG block control E-4031 (n=6) (p=0.0023; One-way ANOVA). **(B)** Comparison of control recordings taken at the start of everyday. **(C)** Dose response curve for all Ziram conditions, mean plotted as red square.
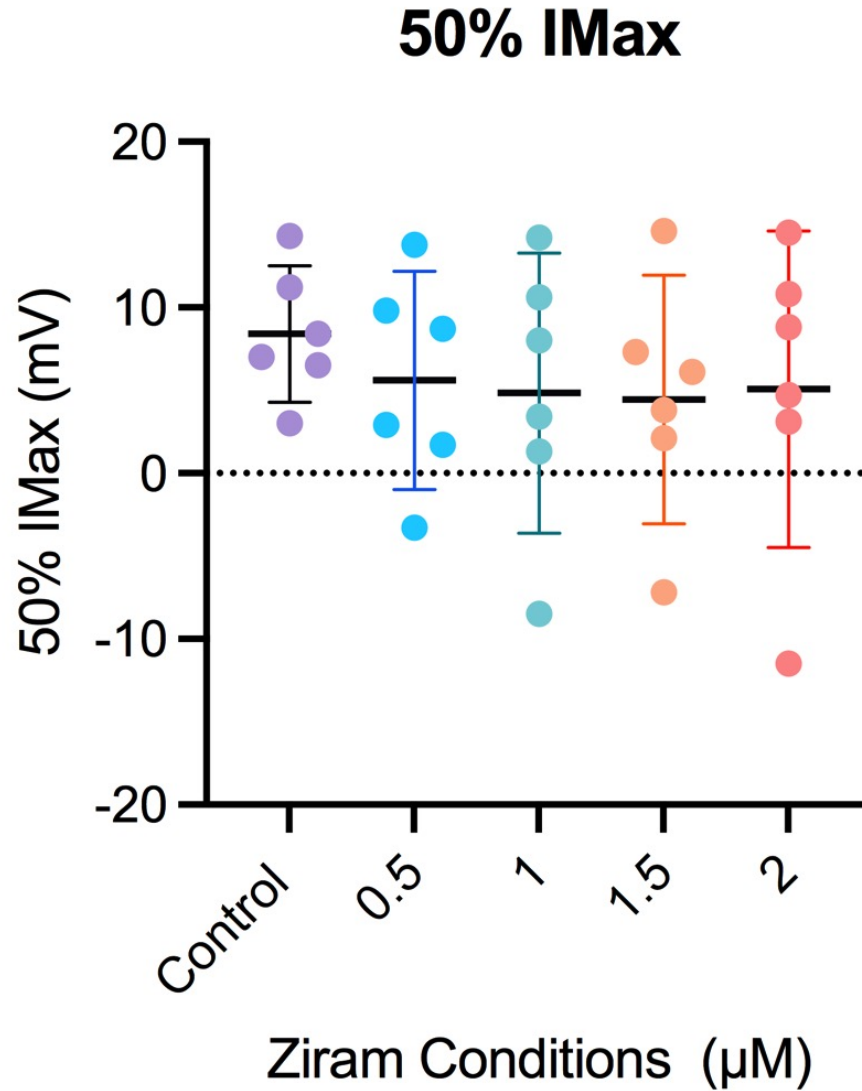
Figure 3. Ziram does not affect 50% IMAX. Graph depicting the voltage in millivolts at which each cell reached 50% of its peak current amplitude in picoamps. n=6. Data are represented as the mean and 95% confidence intervals.
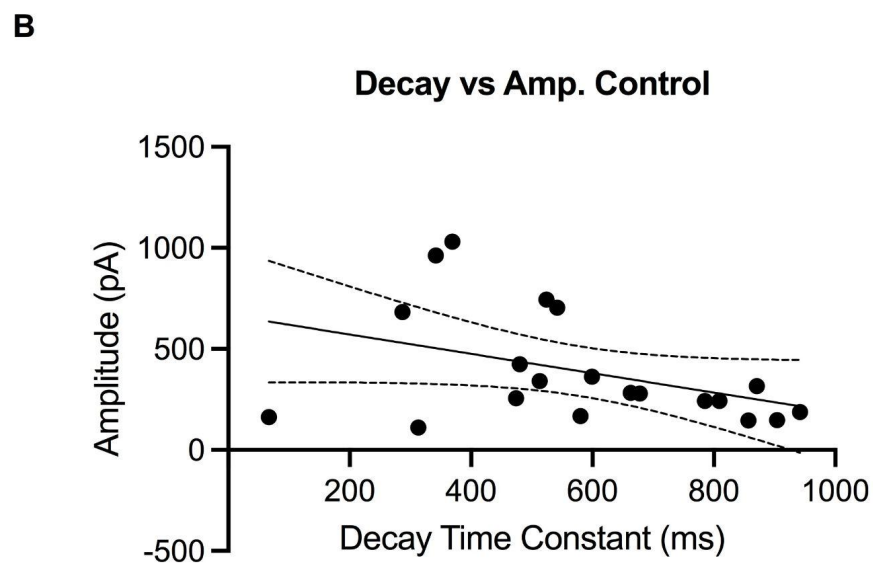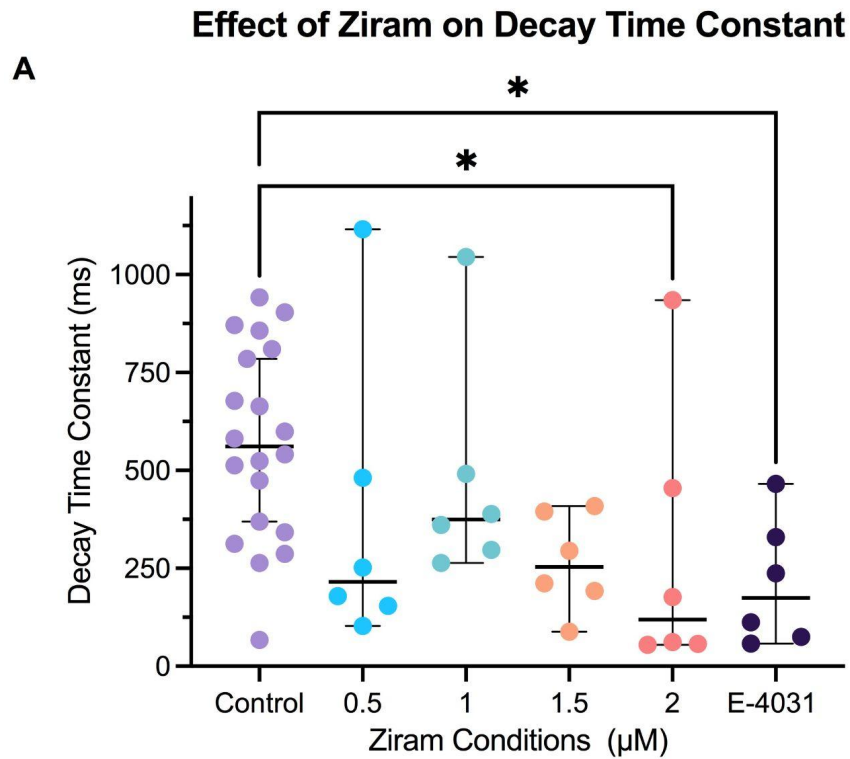
Figure 4. Ziram increases the rate of tail current decay. (A) Ziram at 2uM significantly decreases the decay time constant in a Dunn's multiple comparison test (p=0.038) similar to the effect from E-4031 (p=0.020). **(B)** There is not a significant relationship between tail current amplitude and decay time constant using a simple linear regression (n=20; $R^2 = 0.16$ p > 0.05).

References

Benhorin, J., & Medina, A. (1997). Congenital long-QT syndrome. *New England Journal of Medicine*, *336*(22), 1568–1568. https://doi.org/10.1056/nejm199705293362205

Butler, A., Helliwell, M. V., Zhang, Y., Hancox, J. C., & Dempsey, C. E. (2020). An update on the structure of herg. *Frontiers in Pharmacology*, *10*. https://doi.org/10.3389/fphar.2019.01572

Carson, R. (1962). *Silent spring*. Houghton Mifflin.

Chiesa, N., Rosati, B., Arcangeli, A., Olivotto, M., & Wanke, E. (1997). A novel role for HERG K+channels: Spike-frequency adaptation. *The Journal of Physiology*, *501*(2), 313–318. https://doi.org/10.1111/j.1469-7793.1997.313bn.x

Chou, A. P., Maidment, N., Klintenberg, R., Casida, J. E., Li, S., Fitzmaurice, A. G., Fernagut, P.-O., Mortazavi, F., Chesselet, M.-F., & Bronstein, J. M. (2008). Ziram causes dopaminergic cell damage by inhibiting E1 ligase of the Proteasome. *Journal of Biological Chemistry*, *283*(50), 34696–34703. https://doi.org/10.1074/jbc.m802210200

Curran, M. E., Splawski, I., Timothy, K. W., Vincen, G. M., Green, E. D., & Keating, M. T. (1995). A molecular basis for cardiac arrhythmia: HERG mutations cause long QT syndrome. *Cell*, *80*(5), 795–803. https://doi.org/10.1016/0092-8674(95)90358-5

Das, R., Steege, A., Baron, S., Beckman, J., & Harrison, R. (2001). Pesticide-related illness among migrant farm workers in the United States. *International Journal of Occupational and Environmental Health*, *7*(4), 303–312. https://doi.org/10.1179/oeh.2001.7.4.303

Deguchi, K., Sasaki, I., Tsukaguchi, M., Kamoda, M., Touge, T., Takeuchi, H., & Kuriyama, S. (2002). Abnormalities of rate-corrected qt intervals in parkinson's disease—a comparison with multiple system atrophy and progressive supranuclear palsy. *Journal of the Neurological Sciences*, *199*(1–2), 31–37. https://doi.org/10.1016/s0022-510x(02)00079-5

Fitzmaurice, A. G., Rhodes , S. L., Cockburn, M., Ritz, B., & Bronstein, J. M. (2014). Aldehyde dehydrogenase variation enhances effect of pesticides associated with parkinson disease. *Neurology*, *83*(20), 1880–1880. https://doi.org/10.1212/wnl.0000000000000996

Harrigan, J., Brambila, D. F., Meera, P., Krantz, D. E., & Schweizer, F. E. (2020). The environmental toxicant ziram enhances neurotransmitter release and increases neuronal excitability via the EAG family of potassium channels. *Neurobiology of Disease*, *143*, 104977. https://doi.org/10.1016/j.nbd.2020.104977

Kamiya, K., Mitcheson, J. S., Yasui, K., Kodama, I., & Sanguinetti, M. C. (2001). Open channel block of HERG K channels by Vesnarinone. *Molecular Pharmacology*, *60*(2), 244–253. https://doi.org/10.1124/mol.60.2.244

Kamiya, K., Niwa, R., Mitcheson, J. S., & Sanguinetti, M. C. (2006). Molecular

determinants of herg channel block. *Molecular Pharmacology*, *69*(5), 1709–1716. https://doi.org/10.1124/mol.105.020990

Kiehn, Johann, et al. (1996). "Molecular Physiology and Pharmacology of HERG." *Circulation*, vol. 94, no. 10, pp. 2572–2579., https://doi.org/10.1161/01.cir.94.10.2572.

Luo, Y., & Zhang, M. (2010). Spatially distributed pesticide exposure assessment in the Central Valley, California, USA. *Environmental Pollution*, *158*(5), 1629–1637. https://doi.org/10.1016/j.envpol.2009.12.008

Martin, C. A., Myers, K. M., Chen, A., Martin, N. T., Barajas, A., Schweizer, F. E., & Krantz, D. E. (2016). Ziram, a pesticide associated with increased risk for Parkinson's disease, differentially affects the presynaptic function of aminergic and glutamatergic nerve terminals at the drosophila neuromuscular junction. *Experimental Neurology*, *275*, 232–241. https://doi.org/10.1016/j.expneurol.2015.09.017

Matthews, G. A. (2018). *A history of pesticides*. CABI.

McPate, M. J., Duncan, R. S., Witchel, H. J., & Hancox, J. C. (2006). Disopyramide is an effective inhibitor of mutant HERG K+ channels involved in variant 1 short QT syndrome. *Journal of Molecular and Cellular Cardiology*, *41*(3), 563–566. https://doi.org/10.1016/j.yjmcc.2006.05.021

Molecular Devices LLC . (2021). *The Axon Guide*. Retrieved December 10, 2021, from http://centers.njit.edu/stglab/sites/stglab/files/The%20axon%20Guide.pdf.

Mostafalou, S., & Abdollahi, M. (2013). Pesticides and human chronic diseases: Evidences, mechanisms, and perspectives. *Toxicology and Applied Pharmacology*, *268*(2), 157–177. https://doi.org/10.1016/j.taap.2013.01.025

Nakajima, T. (1999). Voltage-shift of the current activation in HERG S4 mutation (R534C) in LQT2. *Cardiovascular Research*, *44*(2), 283–293. https://doi.org/10.1016/s0008-6363(99)00195-9

Ooi, Amanda, et al. (2016). "A Guide to Transient Expression of Membrane Proteins in HEK-293 Cells for Functional Characterization." *Frontiers in Physiology*, vol. 7, https://doi.org/10.3389/fphys.2016.00300.

Osman, K. A. (2011). Pesticides and human health. *Pesticides in the Modern World - Effects of Pesticides Exposure*. https://doi.org/10.5772/16516

Perry, Matthew D., et al. (2015). "Getting to the Heart of Herg K+Channel Gating." *The Journal of Physiology*, vol. 593, no. 12, pp. 2575–2585., https://doi.org/10.1113/jp270095.

Ritz, B., & Yu, F. (2000). Parkinson's disease mortality and pesticide exposure in California 1984–1994. *International Journal of Epidemiology*, *29*(2), 323–329.

https://doi.org/10.1093/ije/29.2.323

Sanguinetti, M. C., Jiang, C., Curran, M. E., & Keating, M. T. (1995). A mechanistic link between an inherited and an acquired cardiac arrhythmia: HERG encodes the IKR potassium channel. *Cell*, *81*(2), 299–307. https://doi.org/10.1016/0092-8674(95)90340-2

Schwartz, P. J. (2008). The Long QT Syndrome: A clinical counterpart of hERG mutations. *The hERG Cardiac Potassium Channel: Structure, Function and Long QT Syndrome*, 186–203. https://doi.org/10.1002/047002142x.ch15

Shibasaki, T. (1987). Conductance and kinetics of delayed rectifier potassium channels in nodal cells of the rabbit heart. *The Journal of Physiology*, *387*(1), 227–250. https://doi.org/10.1113/jphysiol.1987.sp016571

Smith, P. L., Baukrowitz, T., & Yellen, G. (1996). The inward rectification mechanism of the HERG cardiac potassium channel. *Nature*, *379*(6568), 833–836. https://doi.org/10.1038/379833a0

Spector, P. S., Curran, M. E., Zou, A., Keating, M. T., & Sanguinetti, M. C. (1996). Fast inactivation causes rectification of the IKR channel. *Journal of General Physiology*, *107*(5), 611–619. https://doi.org/10.1085/jgp.107.5.611

Su, Z., Limberis, J., Souers, A., Kym, P., Mikhail, A., Houseman, K., Diaz, G., Liu, X., Martin, R. L., Cox, B. F., & Gintant, G. A. (2009). Electrophysiologic characterization of a novel herg channel activator. *Biochemical Pharmacology*, *77*(8), 1383–1390. https://doi.org/10.1016/j.bcp.2009.01.015

Titus, S. A., Warmke, J. W., & Ganetzky, B. (1997). The Drosophila erg K+ channel polypeptide is encoded by the seizure locus. *The Journal of Neuroscience*, *17*(3), 875–881. https://doi.org/10.1523/jneurosci.17-03-00875.1997

Trudeau, M. C., Warmke, J. W., Ganetzky, B., & Robertson, G. A. (1995). HERG, a human inward rectifier in the voltage-gated potassium channel family. *Science*, *269*(5220), 92–95. https://doi.org/10.1126/science.7604285

Vandenberg, J., Perry M., *et al.* (2012). hERG K Channels: Structure, Function, and Clinical Significance. Hill Physiological Reviews 92:3, 1393-1478

Wang, Anthony et al. (2011). "Parkinson's disease risk from ambient exposure to pesticides." *European journal of epidemiology* vol. 26,7: 547-55. doi:10.1007/s10654-011-9574-5

Wang, S., Morales, M. J., Liu, S., Strauss, H. C., & Rasmusson, R. L. (1997). Modulation of HERG affinity for E-4031 by [K+]o and C-type inactivation. *FEBS Letters*, *417*(1), 43–47. https://doi.org/10.1016/s0014-5793(97)01245-3

Zhou, Z., Gong, Q., Ye, B., Fan, Z., Makielski, J. C., Robertson, G. A., & January, C. T. (1998). Properties of HERG channels stably expressed in HEK 293 cells studied at

physiological temperature. *Biophysical Journal, 74*(1), 230–241. https://doi.org/10.1016/s0006-3495(98)77782-3